NPS63-80-001

NAVAL POSTGRADUATE SCHOOL
Monterey, California

FORMULATION OF EFFICIENT FINITE

ELEMENT PREDICTION MODELS

by

R. T. Williams and A. L. Schoenstadt

January 1980

Technical Report Period: October 1978-December 1979

Approved for public release; distribution unlimited.

Prepared for: Naval Environmental Prediction Research Facility and Fleet Numerical Oceanographic Center.

NAVAL POSTGRADUATE SCHOOL
Monterey, California 93940

Rear Admiral Tyler F. Dedman
Superintendent

J. R. Borsting
Provost

The work reported herein was supported by the Naval Environmental Prediction Research Facility and the Fleet Numerical Oceanographic Center.

This report was prepared by:

SECURITY CLASSIFICATION OF THIS PAGE (When Data Entered)

REPORT DOCUMENTATION PAGE

READ INSTRUCTIONS BEFORE COMPLETING FORM

1. REPORT NUMBER: NPS63-80-001	2. GOVT ACCESSION NO.
3. RECIPIENT'S CATALOG NUMBER	
4. TITLE (and Subtitle): Formulation of Efficient Finite Element Prediction Models	5. TYPE OF REPORT & PERIOD COVERED: Report for Oct 78 - Dec 79
	6. PERFORMING ORG. REPORT NUMBER
7. AUTHOR(s): R. T. Williams and A. L. Schoenstadt	8. CONTRACT OR GRANT NUMBER(s): N66856-79-WR-79002, N63134-79-WR-90909
9. PERFORMING ORGANIZATION NAME AND ADDRESS: Naval Postgraduate School, Monterey, California 93940	10. PROGRAM ELEMENT, PROJECT, TASK AREA & WORK UNIT NUMBERS
11. CONTROLLING OFFICE NAME AND ADDRESS: Naval Environmental Prediction Research Facility and Fleet Numerical Oceanographic Center, Monterey, California 93940	12. REPORT DATE: January 1980
	13. NUMBER OF PAGES: 37
14. MONITORING AGENCY NAME & ADDRESS (if different from Controlling Office)	15. SECURITY CLASS. (of this report): Unclassified
	15a. DECLASSIFICATION/DOWNGRADING SCHEDULE

16. DISTRIBUTION STATEMENT (of this Report)

Approved for public release; distribution unlimited.

17. DISTRIBUTION STATEMENT (of the abstract entered in Block 20, if different from Report)

18. SUPPLEMENTARY NOTES

19. KEY WORDS (Continue on reverse side if necessary and identify by block number)

Finite Element Method
Numerical Methods
Geostrophic Adjustment

20. ABSTRACT (Continue on reverse side if necessary and identify by block number)

This report compares three finite element formulations of the linearized shallow-water equations which are applied to the geostrophic adjustment process. The three corresponding finite difference schemes are also included in the study. The development follows Schoenstadt (1980) wherein the spatially discretized equations are Fourier transformed in x, and then solved with arbitrary initial conditions. The six schemes are also compared by integrating them numerically from an initial state at

DD FORM 1 JAN 73 1473 EDITION OF 1 NOV 65 IS OBSOLETE
S/N 0102-014-6601

rest with a height perturbation at a single point. The finite difference and finite element primitive equation schemes with unstaggered grid points give very poor results for the small scale features. The staggered scheme B gives much better results with both finite differences and finite elements. The vorticity-divergence system with unstaggered points also is very good with finite differences and finite elements. It is especially important to take into account these results when formulating efficient finite element prediction models.

ABSTRACT

This report compares three finite element formulations of the linearized shallow-water equations which are applied to the geostrophic adjustment process. The three corresponding finite difference schemes are also included in the study. The development follows Schoenstadt (1980) wherein the spatially discretized equations are Fourier transformed in x, and then solved with arbitrary initial conditions. The six schemes are also compared by integrating them numerically from an initial state at rest with a height perturbation at a single point. The finite difference and finite element primitive equation schemes with unstaggered grid points give very poor results for the small scale features. The staggered scheme B gives much better results with both finite differences and finite elements. The vorticity-divergence system with unstaggered points also is very good with finite differences and finite elements. It is especially important to take into account these results when formulating efficient finite element prediction models.

TABLE OF CONTENTS

1. Introduction

The finite element method (FEM), which was developed in engineering statics, has recently been introduced into various atmospheric prediction models (Cullen, 1974; Hinsman, 1975; Staniforth and Mitchell, 1977). The FEM is a special case of the Galerkin procedure in which the dependent variables are approximated by a finite sum of spatially varying basis functions with time dependent coefficients. The FEM basis functions are low order polynomials which are zero except in a localized region. The Galerkin procedure produces a set of coupled ordinary differential equations for the coefficients which are solved by introducing finite differences in time (see for example Pinder and Gray (1977)).

FEM models are potentially more accurate than finite difference models, but they normally require more computational effort per degree of freedom. For this reason it is especially important to formulate FEM models efficiently. Kelley and Williams (1976) found considerable small scale noise in an FEM model of the shallow water equations in a channel which had all variables carried at the same nodal points. Winninghoff (1968), Arakawa and Lamb (1977) and Schoenstadt (1980) have demonstrated the advantages of spatial staggering of dependent variables in finite difference models. Also Staniforth and Mitchell (1977, 1978) have obtained excellent results with a vorticity-divergence FEM formulation. This paper will compare these FEM formulations by considering the geostrophic adjustment process with the linearized shallow water equations in one dimension.

2. Basic Equations

The linearized shallow-water equations with no mean flow can be written:

$$\frac{\partial u}{\partial t} - fv + g\frac{\partial h}{\partial x} = 0 \ , \tag{2.1}$$

$$\frac{\partial v}{\partial t} + fu = 0 \ , \tag{2.2}$$

$$\frac{\partial h}{\partial t} + H\frac{\partial u}{\partial x} = 0 \ , \tag{2.3}$$

where u and v are the perturbation velocities in the x and y directions, respectively, and H and h the mean and perturbed heights of the free surface. Also g represents gravity and f is the coriolis parameter. Note that all quantities are independent of y.

The vorticity and divergence equations are obtained by differentiating (2.1) and (2.2) with respect to x which yields:

$$\frac{\partial D}{\partial t} - f\zeta + g\frac{\partial^2 h}{\partial x^2} = 0 \ , \tag{2.4}$$

$$\frac{\partial \zeta}{\partial t} + fD = 0 \ , \tag{2.5}$$

$$\frac{\partial h}{\partial t} + HD = 0 \ , \tag{2.6}$$

where $D = \partial u/\partial x$ is the divergence and $\zeta = \partial v/\partial x$ is the vorticity. These relations for D and ζ are particularly simple in this case since $\partial u/\partial y = \partial v/\partial y = 0$.

Schoenstadt (1977) solved the continuous equations (2.1)-(2.3) with the of the spatial Fourier transform. If we denote Fourier transforms by a tilde, such as

$$\tilde{u}(k,t) = \int_{-\infty}^{\infty} u(x,t)\, e^{-ikx}\, dx \,, \tag{2.7}$$

then the set (2.1)-(2.3) can be transformed to the form:

$$\frac{d\tilde{u}}{dt} = \eta f \tilde{v} - i\mu g \tilde{h} \,, \tag{2.8}$$

$$\frac{d\tilde{v}}{dt} = -\eta f \tilde{u} \,, \tag{2.9}$$

$$\frac{d\tilde{h}}{dt} = -i\mu H \tilde{u} \,, \tag{2.10}$$

where $\eta = 1$ and $\mu = k$. The quantities η and μ will be useful later when finite difference and finite element solutions are needed. The initial conditions are written

$$\tilde{u}_0 = \tilde{u}(k,0) = \int_{-\infty}^{\infty} u(x,0)\, e^{-ikx}\, dx \,, \tag{2.11}$$

with similar definitions for $\tilde{v}_o$ and $\tilde{h}_o$. Schoenstadt (1977) solved the set (2.7)-(2.9) subject to initial conditions by the eigenvalue-eigenvector approach which gives:

$$\tilde{u}(k,t) = \tilde{u}_o \cos \nu t + \eta f \frac{\tilde{v}_o}{\nu} \sin \nu t - \frac{i\mu g h_o}{\nu} \sin \nu t \,, \tag{2.12}$$

$$\tilde{v}(k,t) = -\frac{\eta f}{\nu} \tilde{u}_o \sin \nu t + \{\frac{\mu^2 gH}{\nu^2} + \frac{\eta^2 f^2}{\nu^2} \cos \nu t\} \tilde{v}_o + \frac{ig\mu\eta f}{\nu^2} \{1 - \cos \nu t\} \tilde{h}_o \,, \tag{2.13}$$

$$\tilde{h}(k,t) = -\frac{i\mu H}{\nu} \tilde{u}_o \sin \nu t - \frac{i\mu\eta f H}{\nu^2} \{1 - \cos \nu t\} \tilde{v}_o + \{\frac{\eta^2 f^2}{\nu^2} + \frac{\mu^2 gH}{\nu^2} \cos \nu t\} \tilde{h}_o \,, \tag{2.14}$$

where:

$$\nu^2 = \eta^2 f^2 + \mu^2 gH \,. \tag{2.15}$$

The transformed vorticity-divergence set (2.4)-(2.6) is written:

$$\frac{d\tilde{D}}{dt} - f\tilde{\zeta} - \mu^2 g\tilde{h} = 0 \ , \tag{2.16}$$

$$\frac{d\tilde{\zeta}}{dt} + f\tilde{D} = 0 \ , \tag{2.17}$$

$$\frac{d\tilde{h}}{dt} + H\tilde{D} = 0 \ , \tag{2.18}$$

where $\mu^2 = k^2$. The solution to this set, which can be obtained directly or by using $\tilde{D} = iku$ and $\tilde{\zeta} = ikv$ in (2.13)-(2.15), is given by:

$$\tilde{D}(k,t) = \tilde{D}_o \cos \nu t + \frac{f\tilde{\zeta}_o}{\nu} \sin \nu t + \frac{\mu^2 g h_o}{\nu} \sin \nu t \ , \tag{2.19}$$

$$\tilde{\zeta}(k,t) = -\frac{f\tilde{D}_o}{\nu} \sin \nu t + \left[\frac{\mu^2 gH}{\nu^2} + \frac{f^2}{\nu^2} \cos \nu t \right] \tilde{\zeta}_o - \frac{\mu^2 f}{\nu^2} [1 - \cos \nu t] \, g\tilde{h}_o \ , \tag{2.20}$$

$$\tilde{h}(k,t) = -\frac{H\tilde{D}_o}{\nu} \sin \nu t - \frac{Hf}{\nu^2} [1 - \cos \nu t] \, \tilde{\zeta}_o + \left[\frac{f^2}{\nu^2} + \frac{\mu^2 gH}{\nu^2} \cos \nu t \right] \tilde{h}_o \ , \tag{2.21}$$

where: $$\nu^2 = f^2 + \mu^2 gH \ . \tag{2.22}$$

3. Finite Difference and Finite Element Solutions

Schoenstadt (1980) carried out a general analysis of the solutions to (2.1)-(2.3) which allowed for spatially centered finite differences or finite elements. We will use the same method to compare certain finite difference and finite element solutions to systems (2.1)-(2.3) and (2.4)-(2.6). The various finite difference and finite element forms corresponding to (2.1)-(2.3) or (2.4)-(2.6) are given in the Appendix. Following Schoenstadt (1980) the Fourier transformed versions of the various numerical schemes for the equations (2.1)-(2.3) can be written in the following form:

$$\alpha(k)\,\frac{d\tilde{u}}{dt} = f\beta(k)\,\tilde{v} - ig\sigma(k)\,\tilde{h}\ , \tag{3.1}$$

$$\alpha(k)\,\frac{d\tilde{v}}{dt} = -f\beta(k)\,\tilde{u}\ , \tag{3.2}$$

$$\alpha(k)\,\frac{d\tilde{h}}{dt} = -iH\sigma(k)\,\tilde{u}\ . \tag{3.3}$$

The functions $\alpha(k)$, $\beta(k)$ and $\sigma(k)$ are given in Table I for the various schemes considered. This set can be put in the same form as (2.8)-(2.10) by dividing by α and by setting:

$$\eta = \beta/\alpha \quad \text{and} \quad \mu = \sigma/\alpha\ . \tag{3.4}$$

In this case the frequency is given by

$$\nu^2 = (\beta^2 f^2 + \sigma^2 gH)/\alpha^2\ . \tag{3.5}$$

The solutions to set (3.1)-(3.3) are given by (2.12)-(2.14) with the use of (3.4) and (3.5).

Table I. Coefficients in primitive equations for various numerical schemes.

Scheme	α	β	σ
differential	1	1	k
A	1	1	$\sin(k\Delta x)/\Delta x$
B	1	1	$\sin(k\Delta x/2)/(\Delta x/2)$
FEM A	$(2+\cos(k\Delta x))/3$	$(2+\cos(k\Delta x))/3$	$\sin(k\Delta x)/\Delta x$
FEM B	$(2+\cos(k\Delta x))/3$	$(2+\cos(k\Delta x))/3$	$(5\sin(k\Delta x/2)+\sin(3k\Delta x/2))/4\Delta x$

The numerical schemes for the vorticity-divergence system (2.4)-(2.6) lead to the following transformed equations:

$$\alpha \frac{d\tilde{D}}{dt} - \alpha f\tilde{\zeta} - \sigma^2 g\tilde{h} = 0 \ , \tag{3.6}$$

$$\alpha \frac{d\tilde{\zeta}}{dt} + f\alpha\tilde{D} = 0 \ , \tag{3.7}$$

$$\alpha \frac{d\tilde{h}}{dt} + H\alpha\tilde{D} = 0 \ , \tag{3.8}$$

where $\alpha(k)$ and $\sigma(k)$ are given in Table II. This set can be put in the same form as (2.16)-(2.18) by dividing by α and setting:

$$\mu^2 = \sigma^2/\alpha \ . \tag{3.9}$$

The frequency equation (2.22) becomes

$$\nu^2 = f^2 + (\sigma^2/\alpha)gH \ , \tag{3.10}$$

which has a different form from (3.5). The solutions to set (3.6)-(3.8) are given by (3.6)-(3.8) with the use of (3.9) and (3.10).

Table II. Coefficients in vorticity-divergence equations for various numerical schemes.

Scheme	α	σ^2
Scheme differential	1	k^2
finite difference	1	$\sin^2(k\Delta x/2)/(\Delta x/2)^2$
FEM	$(2+\cos(k\Delta x))/3$	$\sin^2(k\Delta x/2)/(\Delta x/2)^2$

The various parameters which determine the solutions (2.13)-(2.15) and (2.19)-(2.21) are shown in Tables I and II, respectively. Table I contains Schemes A and B for the primitive equations where Scheme A is unstaggered and Scheme B has the velocity points midway between the height points (see Schoenstadt, 1980). The table also includes the finite element forms which are obtained when piecewise linear basis functions are used. Note that k is poorly represented by σ with Scheme A near $k = \pi/\Delta x$, and that the problem remains with the FEM version of Scheme A. The staggered grid gives a much better approximation since spatial derivatives are computed over a distance of Δx compared to $2\Delta x$ with the unstaggered grid.

Table II contains the parameters for the finite difference and finite element versions of the vorticity-divergence set of equations. In this case vorticity, divergence and height are carried at the same points. Note that σ^2 for both cases is the same as the value of σ^2 for Scheme B from Table I. It can be seen from the tables that the staggered primitive equation (Scheme B) and vorticity-divergence formulations have the same values for α and σ and therefore for ν, so that these should give the same solution except for truncation error in the initial conditions.

As pointed out by Schoenstadt (1980), the solutions (2.12)-(2.14) for the various schemes differ only through the coefficients η/ν, μ/ν, and $\eta\mu/\nu^2$, and the same dependence occurs in system (2.19)-(2.21) with $\eta = 1$, except that the coefficient $\eta\mu/\nu^2$ does not appear. Figure 1a contains the phase velocity, $c = \nu/k$, as a function of $k\Delta x/\pi$ for the various schemes in Tables I and II as computed from (3.5) and (3.10), respectively. The differential solution approaches f/k for small k and the shallow-water speed $(gH)^{1/2}$ for large k. Scheme A gives the poorest phase speed and the finite element Scheme A is also very poor for the

highest wavenumbers. The finite element scheme B is very close to the differential solution, while the vorticity-divergence FEM scheme is a little higher. The group velocity, $G = d\nu/d\mu$, is given in Fig. 1b, as a function of $k\Delta x/\pi$. The differential solution is zero at $k = 0$ and it approaches the shallow-water phase speed $(gH)^{1/2}$ for large k. Scheme A and its FEM version are very poor for the short waves since they propagate energy in the wrong direction. In fact the FEM scheme gives a group velocity which is more than double the correct value and of the wrong sign, at certain points. The FEM scheme B gives the best group velocity while the FEM vorticity-divergence scheme gives values that are somewhat higher.

The coefficients η/ν, μ/ν and $\eta\mu/\nu^2$ are given in Fig. 2a, 2b and 2c, respectively, as functions of $k\Delta x/\pi$. Scheme A is the poorest for each coefficient, but the FEM version of scheme A is just as bad for the short waves. The best scheme is the FEM version of scheme B, although the FEM vorticity-divergence scheme is also very good. The coefficient η/ν, which is given in Fig. 2a, is especially important since η^2/ν^2 relates the initial height to the final (steady-state) height field (see (2.14)). In particular, the figure shows that if $v_o = 0$, the final h for $k = \pi/\Delta x$ is more than 25 times too large for scheme A and the FEM version of A! This is one reason why non-staggered schemes tend to generate small scale noise. These results were given by Schoenstadt (1980) with the exception of the vorticity-divergence schemes.

4. Final State Example

The two aspects of the geostrophic adjustment process that must be considered in assessing a particular numerical scheme are: 1) forecast time required to reach the adjusted state, 2) the accuracy of the final

adjusted state. The group velocity curves in Fig. 1a provide an indication of the comparative adjustment times for the various schemes. The final adjusted state, which is more important, could be obtained by Fourier transforming the terms that are independent of t in (2.12)-(2.14) or (2.19)-(2.21). However, in this paper the final state will be determined by integrating the finite difference equations in t until the adjusted state is reached. This approach is preferable because time differencing effects are included and a time filter can also be used.

The various sets of equations, which are given in the Appendix are integrated with centered time differences. The time filter developed by Robert (1966) (see also Asselin, 1972) is applied to the past time value with the coefficient $\gamma = .05$. The new time values for the FEM schemes are found by Gauss elimination.

The initial conditions are given by:

$$h(x,o) = \begin{cases} a & |x| \leq \Delta x/2 \\ o & |x| > \Delta x/2 \ , \end{cases} \tag{4.1}$$

$$u(x,o) = v(x,o) = 0 \ , \quad \text{or} \quad \zeta(x,o) = D(x,o) = 0 \ .$$

These initial conditions are convenient for comparing the various schemes since no truncation error is introduced when the initial vorticity and divergence are computed from these initial velocities. The analytic solution for the final adjusted h field can be obtained by integrating the following expression that was obtained by Schoenstadt (1977):

$$h_s(x) = h(x,o) - \frac{H}{2\lambda^2 f} \int_{-\infty}^{\infty} \operatorname{sgn}(x-\xi) e^{-|x-\xi|/\lambda} \left[\frac{g}{f} \frac{\partial h}{\partial x}(\xi,0) - v(\xi,0)\right] d\xi \ , \tag{4.2}$$

where $h_s(x)$ is the final adjusted height and $\lambda = (gH)^{1/2}/f$ is the Rossby radius of deformation. The initial geostrophic wind which is required in (4.2) can be conveniently written:

$$\frac{g}{f}\frac{\partial h}{\partial x}(x,0) = \frac{ag}{f}\left[\delta(x+\Delta x/2)-\delta(x-\Delta x/2)\right] , \qquad (4.3)$$

where $\delta(x)$ is the delta function.

When (4.1) and (4.3) are introduced into (4.2) the solution becomes:

$$h_s(x) = a \begin{cases} e^{-x/\lambda}\sinh(\Delta x/2\lambda) & \Delta x/2 < x \\ 1 - e^{-\Delta x/2\lambda}\cosh(x/\lambda) & -\Delta x/2 \leq x \leq \Delta x/2 \\ e^{x/\lambda}\sinh(\Delta x/2\lambda) & x < -\Delta x/2 \end{cases} . \qquad (4.4)$$

Fig. 3 contains $h_s(x)$ for the case $\Delta x = \lambda/2$.

The numerical integrations with the various schemes are performed on a grid of 200 points with cyclic boundary conditions. The initial disturbance at x = 0 is placed in the center of the computational domain so that the cyclic boundary conditions will not affect the solution near x = 0 until well after the adjusted state is reached. Fig. 3 includes the numerical solutions at t = 3 days for the following schemes: A, B and FEM A. Scheme A shows strong oscillations with every other point returning to 0. The FEM scheme A has smaller oscillations near x = 0, but they become larger than the oscillations with scheme A farther out. Scheme B gives very smooth behavior and it is close to the analytic solution. The vorticity-divergence system gives the same solution as scheme B, and is very close to the analytic solution as can be seen in Table III which compares the solutions at the first two grid points.

Table III. Numerical solutions h/a at t = 72 hours for the first two grid points for various schemes compared with analytic solution.

x	0	Δx
Differential	0.221	0.153
A	0.459	0.0
B	0.240	0.148
vorticity-divergence	0.240	0.148
FEM A	0.298	0.084
FEM B	0.227	0.157
FEM vorticity-divergence	0.213	0.154

The results given in Fig. 3 and Table III are consistent with the curves for η/ν shown in Fig. 2a, since h_s is proportional to η^2/ν^2 (see (2.14) and (2.21)). In particular the poor behavior for the unstaggered primitive equation schemes (A and FEM A) in Fig. 2a is consistent with the large amplitude short waves in Fig. 3. Also the large oscillations farther out with FEM A may be the result of the large spurious group velocity that is shown in Fig. 1b for that scheme. All the staggered primitive equation and vorticity-divergence schemes give excellent predictions of the final adjusted height field. It should be pointed out that the inclusion of light time smoothing (γ = .05) is necessary to produce the spatially smooth solutions for these cases. Apparently the vanishing group velocity for $k\Delta x/\pi = 1$ (see Fig. 1b) does not allow the smallest scale gravity waves to propagate out from the initial disturbance. Haltiner and McCollough (1975) demonstrated the usefulness of time filtering in a baroclinic primitive equation model.

5. Conclusions

The objective of this paper is to determine the response of various finite element schemes to small scale initial conditions or small scale forcing. It is especially important that FEM prediction schemes properly describe small scale features, because FEM models usually require more computational effort per degree of freedom than most finite difference models. This study treated the geostrophic adjustment process with the linearized primitive equations and also with the related vorticity-divergence set of equations. The development followed Schoenstadt (1980) wherein the spatially discretized equations were Fourier transformed in x, and then solved with arbitrary initial conditions. These solutions were dependent on certain coefficients which were computed for the various numerical schemes and compared with the differential expressions. Three FEM schemes were examined as well as the three corresponding finite difference schemes. It was found that the unstaggered (scheme A) primitive equation model gives the poorest behavior followed by the corresponding FEM formulation. These schemes are especially bad for the shortest resolvable scales. The finite difference primitive equation model, which staggers height points between velocity points (scheme B) has much better behavior than the unstaggered schemes. The vorticity-divergence model where ζ, D and h are carried at the same points has the same coefficients as scheme B. The FEM version of scheme B, which has staggered nodal points, was found to have the best behavior and the FEM vorticity-divergence model was also found to be very good.

The six schemes were also compared by integrating them numerically with centered time differences from an initial state at rest with a height perturbation at a single point. The analytic solution for this initial

state approached a smooth height field after the inertial gravity waves radiated away. Scheme A and the FEM form of scheme A gave very poor solutions with large oscillations from point to point. All of the other schemes produced smooth solutions with the FEM schemes being the most accurate. The smoothness of these solutions was improved by light time smoothing. Although the initial state used in this comparison is somewhat extreme, it shows clearly the superiority of the staggered primitive equation and vorticity-divergence schemes over the non-staggered primitive equation schemes.

Winninghoff (1968), Arakawa and Lamb (1977) and Schoenstadt (1980) have demonstrated the advantages of spatial staggering of predictive variables in finite difference models. Our results strongly indicate that FEM models should either use staggered nodal points in the primitive equations or unstaggered nodal points in the vorticity-divergence equations (see also Schoenstadt, 1980). In fact Staniforth and Mitchell (1977, 1978) have developed a FEM model based on the vorticity-divergence form of the shallow-water equations that produces smooth forecasts with only time smoothing. In contrast, Kelley and Williams (1976) obtained very noisy results with an unstaggered FEM model which used the primitive equations for flow in a channel. If non-staggered finite FEM element models are used, it is often necessary to use high order smoothing to damp the small scales as discussed by Cullen (1976). Thacker (1978) tested a finite element formulation of the linearized shallow-water equations with staggered nodal points and he obtained smooth solutions.

Since FEM models usually require more computer time per degree of freedom, it is very important for the numerical scheme used to be accurate for as small a scale as possible. In this paper we have shown that the

usual non-staggered FEM formulation of the primitive equations gives very poor geostrophic adjustment for small scale initial conditions. The same conclusion follows for small scale heating. On the other hand either the use of the primitive equations with staggered nodal points or the vorticity-divergence equations with unstaggered nodal points gives excellent treatment of small scale features in the geostrophic adjustment process. Clearly, the use of either formulation should be much more efficient than the unstaggered primitive equations, even when the latter have smoothing to destroy the smallest scale features.

REFERENCES

Arakawa, A. and V. Lamb, 1977: Computational design of the basic dynamical processes of the UCLA General Circulation Model. Methods of Computational Physics, Academic Press, 17, 174-266.

Asselin, R., 1972: Frequency filter for time interpolations. Mon. Wea. Rev., 100, 487-490.

Cullen, M.J.P., 1974: Integration of the primitive equations on a sphere using the finite element method. Quart. J. R. Met. Soc., 100, 555-562.

_____, 1976: On the use of artificial smoothing in Galerkin and finite difference solutions of the primitive equations. Quart. J. R. Met. Soc., 102, 77-93.

Haltiner, G. J. and J. McCollough, 1975: Experiments in the initialization of a global primitive equation model. J. Appl. Meteor., 14, 281-288.

____, and R. T. Williams, 1980: Numerical Prediction and Dynamic Meteorology. John Wiley and Sons, Inc.

Hinsman, D. E., 1975: Application of a Finite Element Method to the Barotropic Primitive Equations. M.S. Thesis, Naval Postgraduate School, Monterey, California, 116 pp.

Kelley, R. G. and R. T. Williams, 1976: A Finite Element Prediction Model with Variable Element Sizes. Naval Postgraduate School Report, NPS-63Wu76101, 109 pp.

Pinder, G. F. and W. G. Gray, 1977: Finite Element Simulation in Surface and Subsurface Hydrology. Academic Press, New York, 295 pp.

Robert, A., 1966: The integration of a low order spectral form of the primitive meteorological equations. J. Meteor. Soc. Japan, 44, 237-245.

Schoenstadt, A., 1977: The effect of spatial discretization on the steady-state and transient behavior of a dispersive wave equation. J. Comp. Phys., 23, 364-379.

_____, 1980: A transfer function analysis of numerical schemes used to simulate geostrophic adjustment. Mon. Wea. Rev., 108.

Staniforth, A. N., and H. L. Mitchell, 1977: A semi-implicit finite-element barotropic model. Mon. Wea. Rev., 105, 154-169.

_____, 1978: A variable-resolution finite-element technique for regional forecasting with the primitive equations. Mon. Wea. Rev., 106, 439-447.

Thacker, W. C., 1978: Comparison of finite-element and finite-difference schemes. Part I: One-dimensional gravity wave motion. J. Phys. Oceanogr., 8, 676-679.

Winninghoff, F., 1968: On the Adjustment Toward a Geostrophic Balance in a Simple Primitive Equation Model with Application to the Problem on Initialization and Objective Analysis. Doctoral Dissertation, UCLA, pp 161.

Appendix

In this Appendix the spatially discretized prediction equations are given for each scheme with $x = m\Delta x$. The following schemes approximate the primitive equations (2.1)-(2.3):

Scheme A

$$\frac{\partial u_m}{\partial t} - f v_m + \frac{g(h_{m+1} - h_{m-1})}{2\Delta x} = 0 ,$$

$$\frac{\partial v_m}{\partial t} + f u_m = 0 ,$$

$$\frac{\partial h_m}{\partial t} + H \left(\frac{u_{m+1} - u_{m-1}}{2\Delta x}\right) = 0 .$$

FEM Scheme A

$$M \frac{\partial u_m}{\partial t} - f\, M v_m + \frac{g(h_{m+1} - h_{m-1})}{2\Delta x} = 0 ,$$

$$M \frac{\partial v_m}{\partial t} + f\, M u_m = 0 ,$$

$$M \frac{\partial h_m}{\partial t} + H \left(\frac{u_{m+1} - u_{m-1}}{2\Delta x}\right) = 0 .$$

Scheme B

$$\frac{\partial u_m}{\partial t} - f v_m + \frac{g(h_{m+1/2} - h_{m-1/2})}{\Delta x} = 0 ,$$

$$\frac{\partial v_m}{\partial t} + f u_m = 0 ,$$

$$\frac{\partial h_m}{\partial t} + H\left(\frac{u_{m+1/2} - u_{m-1/2}}{\Delta x}\right) = 0 .$$

FEM Scheme B

$$M\frac{\partial u_m}{\partial t} - fMv_m + \frac{5}{8}\left(\frac{h_{m+1/2} - h_{m-1/2}}{\Delta x}\right) + \frac{3}{16}\left(\frac{h_{m+1/2} - h_{m-1/2}}{\Delta x}\right) = 0 ,$$

$$M\frac{\partial v_m}{\partial t} + fMu_m = 0 ,$$

$$M\frac{\partial h_m}{\partial t} + H\left[\frac{5}{8}\left(\frac{u_{m+1/2} - u_{m-1/2}}{\Delta x}\right) + \frac{3}{8}\left(\frac{u_{m+3/2} - u_{m-3/2}}{\Delta x}\right)\right] = 0 ,$$

where $M\alpha_m = (\alpha_{m+1} + 4\alpha_m + \alpha_{m-1})/6$.

Scheme B is staggered in such a way that the height points are equi-distant between the velocity points. The FEM equations can be derived with piecewise linear basis functions (see for example Chapter 6 in Haltiner and Williams, 1980).

The vorticity-divergence system (2.4)-(2.6) is approximated with the following schemes.

Vorticity-Divergence

$$\frac{\partial D_m}{\partial t} - f\zeta_m + g\left(\frac{h_{m+1} - 2h_m + h_{m-1}}{\Delta x^2}\right) = 0 ,$$

$$\frac{\partial \zeta_m}{\partial t} + fD_m = 0 ,$$

$$\frac{\partial h_m}{\partial t} + HD_m = 0 .$$

Finite Element Vorticity-Divergence

$$M\frac{\partial D_m}{\partial t} - fM\zeta_m + g\frac{h_{m+1} - 2h_m + h_{m-1}}{\Delta x^2} = 0 ,$$

$$M\frac{\partial \zeta_m}{\partial t} + fMD_m = 0 ,$$

$$M\frac{\partial h_m}{\partial t} + HMD_m = 0 .$$

Figure Captions

Fig. 1. The phase velocity $c = \nu/\mu$, and the group velocity $G = d\nu/d\mu$ as functions of $k\Delta x/\pi$ for various numerical schemes. The curves are labeled as follows: 1) differential solution, 2) scheme A, 3) scheme B and vorticity divergence finite difference scheme, 4) FEM scheme A, 5) FEM scheme B, 6) FEM vorticity-divergence scheme. These results use the following values: $gH = 10^4\ m^2s^{-2}$, $f = 10^{-4}s^{-1}$, $\Delta x = 500$ km.

Fig. 2. The coefficients η/ν, μ/ν and $\eta\mu/\nu^2$ as functions of $k\Delta x/\pi$, with the same labeling as in Fig. 1.

Fig. 3. The numerical solutions for schemes A, B and FEM A as functions of $x/\Delta x$ at $t = 3$ days. The steady-state differential solution, which is given by (4.4), is included for comparison.

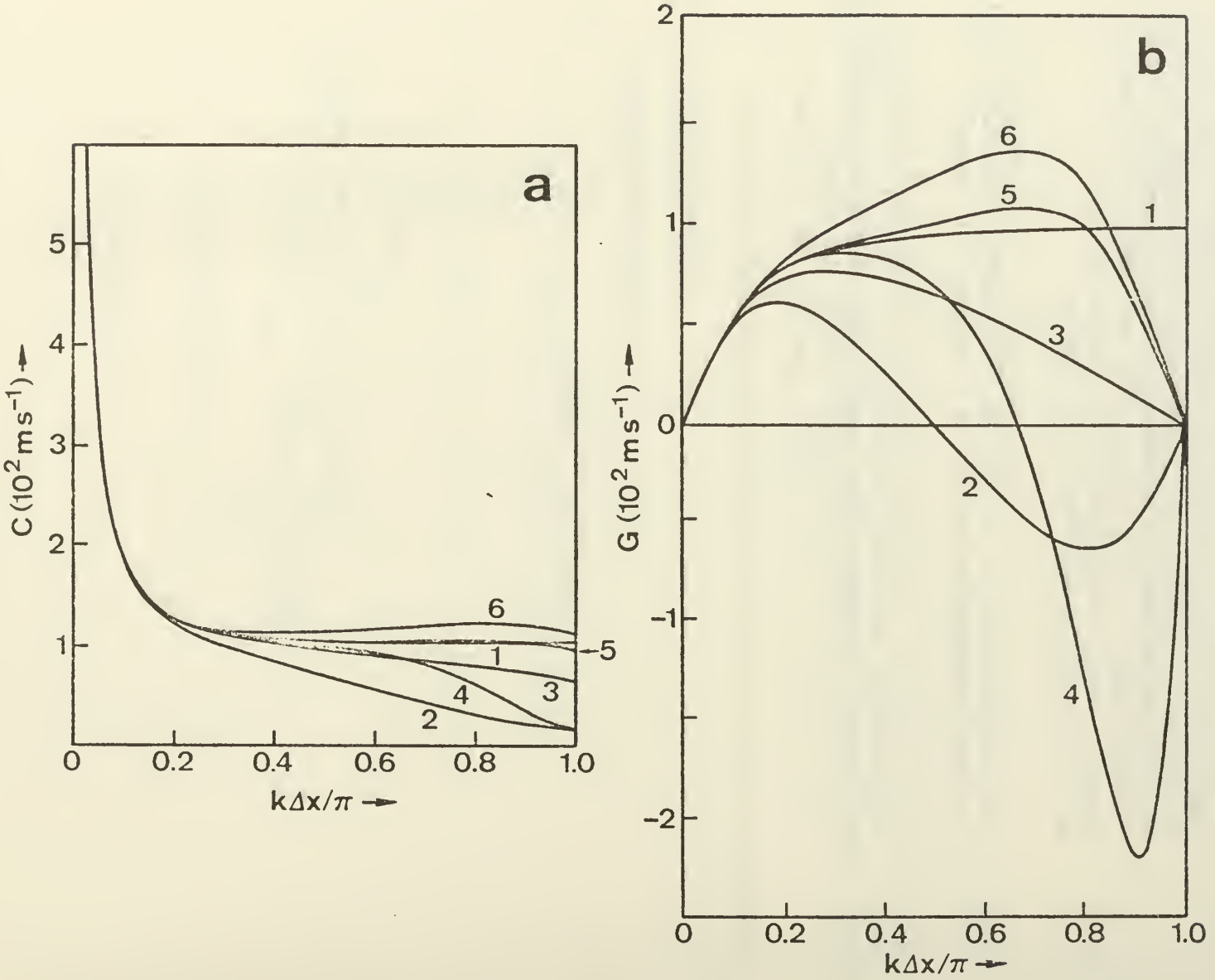

FIGURE 1.

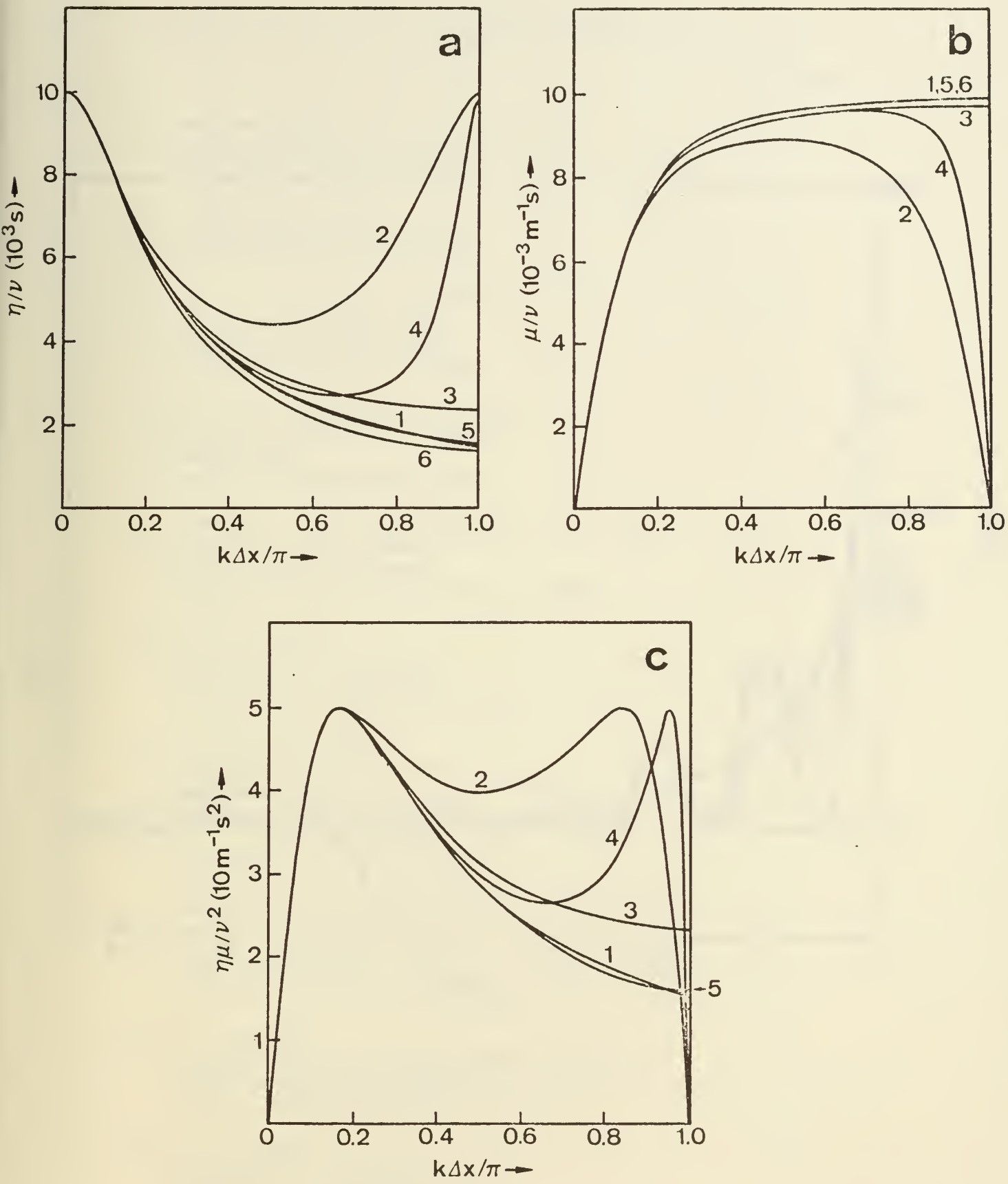
a
b
c
η/ν (10^3s)
μ/ν (10^{-3}m^{-1}s)
$\eta\mu/\nu^2$ (10m^{-1}s^2)
kΔx/π
1,5,6
2
3
4
5
6

FIGURE 2.

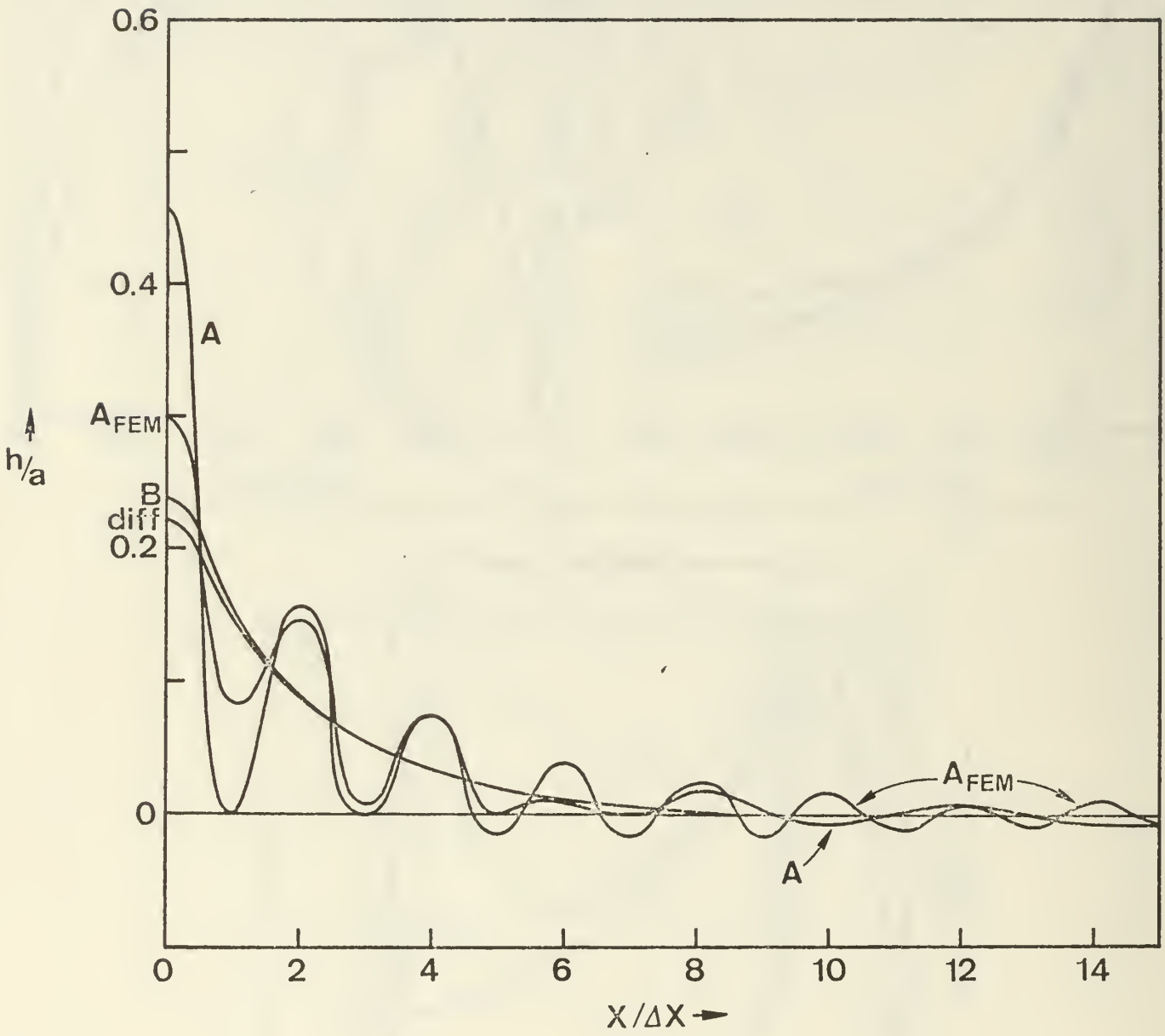

FIGURE 3.

DISTRIBUTION LIST

		No. Copies
1.	Defense Technical Information Center Cameron Station Alexandria, Virginia 22314	2
2.	Library, Code 0142 Naval Postgraduate School Monterey, California 93940	2
3.	Dr. R. T. Williams, Code 63Wu Department of Meteorology Naval Postgraduate School Monterey, California 93940	15
4.	Air Force Geophysics Laboratory Exchange Library Sulls Stop 29 Hanscom AFB Bedford, Massachusetts 01730	1
5.	Commander, Air Weather Service Military Airlift Command United States Air Force Scott Air Force Base, Illinois 62226	1
6.	Dr. A. Arakawa Department of Meteorology University of California Los Angeles, California 90024	1
7.	Dr. David A. Archer Douglas DuPont Rachford, Inc. 6150 Chevy Chase Houston, Texas 77027	1
8.	Atmospheric Sciences Library National Oceanic and Atmospheric Administration Silver Spring, Maryland 20910	1
9.	Dr. E. Barker Naval Environmental Prediction Research Facility Monterey, California 93940	1
10.	Dr. Tom Beer Western Australian Institute of Technology Hayman Road South Bentley Western Australia 6102	1
11.	Dr. W. Blumen Department of Astro-Geophysics University of Colorado Boulder, Colorado 80302	1

12. Dr. F. P. Bretherton — 1
National Center for Atmospheric Research
P.O. Box 3000
Boulder, Colorado 80303

13. Prof. Dr. Jurgen Brickmann — 1
Universitat Konstanz, Fachbereich Chemie
775 Konstanz
Postfach 77 33, West Germany

14. Dr. John Brown — 1
National Meteorological Center/NOAA
World Weather Building
Washington, D.C. 20233

15. Dr. C.-P. Chang, Code 63Cp — 1
Department of Meteorology
Naval Postgraduate School
Monterey, California 93940

16. Prof. J. G. Charney — 1
54-1424
Massachusetts Institute of Technology
Cambridge, Massachusetts 02139

17. Dr. M.J.P. Cullen — 1
Meteorological Office
Bracknell, Berks, United Kingdom

18. Dean of Research, Code 012 — 2
Naval Postgraduate School
Monterey, California 93940

19. Dr. Tom Delmer — 1
Sciences Applications, Inc.
P.O. Box 2351
La Jolla, California 92037

20. Department of Oceanography, Code 68 — 1
Naval Postgraduate School
Monterey, California 93940

21. Dr. D. Dietrick — 1
JAYCOR
205 S. Whiting St., Suite 409
Alexandria, Virginia 22304

22. Dr. Hugh W. Ellsaesser — 1
Lawrence Livermore Laboratory
P.O. Box 808
Livermore, California 94550

23. Dr. R. L. Elsberry, Code 63Es — 1
Department of Meteorology
Naval Postgraduate School
Monterey, California 93940

24. Prof. F. D. Faulkner, Code 53Fa — 1
Department of Mathematics
Naval Postgraduate School
Monterey, California 93940

25. Commanding Officer — 10
Fleet Numerical Oceanographic Center
Monterey, California 93940

26. Dr. Richard Franke, Code 53Fe — 1
Department of Mathematics
Naval Postgraduate School
Monterey, California 93940

27. Dr. J. A. Galt — 1
NOAA - Pac Mar Envir Lab
University of Washington
Seattle, Washington 98105

28. Dr. W. L. Gates — 1
Department of Meteorology
Oregon State University
Corvallis, Oregon 97331

29. Dr. Ian Gladwell — 1
Department of Mathematics
University of Manchester
Manchester M13 9PL, England
United Kingdom

30. Dr. Earl Gossard — 1
Wave Propagation Laboratory
NOAA/ERL
Boulder, Colorado 80302

31. Dr. G. J. Haltiner, Code 63Ha — 1
Chairman, Department of Meteorology
Naval Postgraduate School
Monterey, California 93940

32. Dr. R. L. Haney, Code 63Hy — 1
Department of Meteorology
Naval Postgraduate School
Monterey, California 93940

33. Captain John L. Hayes — 1
Air Force Global Weather Central
PSC #2, Box 7141
Offutt AFB, Nebraska 68113

34. Dr. J. C. Heinrich 1
Case Western Reserve University
Department of Early Sciences
Cleveland, Ohio 44106

35. Dr. D. Narayana Holla 1
Department of Mathematics
Indian Institute of Technology, Bombay
P.O., I.I.T. Bombay
Powai, Bombay 400 076, India

36. Dr. J. Holton 1
Department of Atmospheric Sciences
University of Washington
Seattle, Washington 98105

37. Dr. W. Horsthemke 1
Universite Libre De Bruxelles-Faculte Des Sci.
Service De Chimie Physique II-Prof. Prigogine
C.P. 231 Campus Plaine-Bd. du Triomphe
1050 Bruxelles, Belgium

38. Dr. B. J. Hoskins 1
Department of Geophysics
University of Reading
Reading, United Kingdom

39. Dr. D. Houghton 1
Department of Meteorology
University of Wisconsin
Madison, Wisconsin 53706

40. Dr. Dennis C. Jespersen 1
Department of Mathematics
Oregon State University
Corvallis, Oregon 97331

41. Dr. E. J. Kansh 1
U.S. Department of the Interior
Bureau of Mines
Pittsburgh, Pennsylvania 15213

42. Dr. S. K. Kao 1
Department of Meteorology
University of Utah
Salt Lake City, Utah 84112

43. Dr. A. Kasahara 1
National Center for Atmospheric Research
P.O. Box 3000
Boulder, Colorado 80303

44. Dr. L. D. Kovach, Code 53Kv — 1
Department of Mathematics
Naval Postgraduate School
Monterey, California 93940

45. Dr. Ing. J. Kumicak — 1
Institute of Radioecology and
Applied Nuclear Techniques
Komenskeho 9, P.O. Box A-41
040 61 Kosice, CSSR Czechoslovakia

46. Dr. Robert L. Lee — 2
Atmospheric and Geophysical Sciences Division
University of California
P.O. Box 808
Livermore, California 94550

47. Dr. C. E. Leith — 1
National Center for Atmospheric Research
P.O. Box 3000
Boulder, Colorado 80303

48. Dr. J. M. Lewis — 1
Laboratory for Atmospheric Research
University of Illinois
Urbana, Illinois 61801

49. Dr. Mei-Kao Liu — 1
System Applications, Inc.
950 Northgate Drive
San Rafael, California 94903

50. Dr. E. N. Lorenz — 1
Department of Meteorology
Massachusetts Institute of Technology
Cambridge, Massachusetts 02139

51. Lieutenant Olaf M. Lubeck — 1
COMNAVMARIANAS, Box 12
FPO San Francisco 96630

52. Dr. F. Ludwikow — 1
Medical School Department of Biophysics
ul. Chalubinskiego 10,
50-368 Wroclaw, Poland

53. Dr. Leon Lupidus — 1
Princeton University
School of Engineering/Applied Science
The Engineering Quadrangle
Princeton, New Jersey 08540

54. Dr. R. Madala, Code 6780 — 1
Naval Research Laboratories
Washington, D.C. 20375

55. Dr. J. D. Mahlman — 1
Geophysical Fluid Dynamics Laboratory
Princeton University
Princeton, New Jersey 08540

56. Dr. Alsan Meric — 1
Applied Mathematics Division
Marmara Research Institute
P.K. 141, Kadikoy
Istanbul, Turkey

57. Meteorology Library, Code 63 — 1
Naval Postgraduate School
Monterey, California 93940

58. Dr. G. Morris, Code 53Mj — 1
Department of Mathematics
Naval Postgraduate School
Monterey, California 93940

59. Prof. J. L. Morris — 1
Computer Science
University of Waterloo
Waterloo, Ontario, Canada

60. National Center for Atmospheric Research — 1
P.O. Box 1470
Boulder, Colorado 80302

61. Officer in Charge — 10
Naval Environmental Prediction Research Facility
Monterey, California 93940

62. Naval Oceanographic Office — 1
Library, Code 3330
Washington, D.C. 20373

63. Commander — 1
Naval Oceanography Command
National Space Technology Laboratories
Bay St Louis, Mississippi 39520

64. Director, Naval Research Laboratory — 1
Attn: Technical Services Information Center
Washington, D.C. 20390

65. Office of Naval Research — 1
Department of the Navy
Washington, D.C. 20360

66. Dr. T. Ogura 1
Laboratory for Atmospheric Research
University of Illinois
Urbana, Illinois 61801

67. Prof. K. Ooyama 1
National Center for Atmospheric Research
P.O. Box 3000
Boulder, Colorado 80303

68. Dr. I. Orlanski 1
Geophysical Fluid Dynamics Laboratory
Princeton University
Princeton, New Jersey 08540

69. Prof. H. D. Orville 1
Institute of Atmospheric Sciences
South Dakota School of Mines and Technolgoy
Rapid City, South Dakota 57701

70. Dr. Darrell W. Pepper 1
Environ. Transport Division
E. I. du Pont de Nemours & Co., Inc.
Savannah River Laboratory
Aiken, South Carolina 29801

71. Prof. N. A. Phillips 1
National Meteorological Center/NOAA
World Weather Building
Washington, D.C. 20233

72. Dr. S. Piacsek 1
NORDA 320
NSTL Station, Mississippi 39529

73. Dr. A. P. Raiche 1
Minerals Reserach Laboratories, CSIRO
P.O. Box 136
North Ryde, NSW 2113, Australia

74. Dr. T. Rosmond 3
Naval Environmental Prediction Research Facility
Monterey, California 93940

75. Prof. D. Salinas, Code 69Zc 1
Department of Mechanical Engineering
Naval Postgraduate School
Monterey, California 93940

76. Dr. Y. Sasaki 1
Department of Meteorology
University of Oklahoma
Norman, Oklahoma 73069

77. Prof. A. L. Schoenstadt, Code 53Zh — 10
Department of Mathematics
Naval Postgraduate School
Monterey, California 93940

78. Prof. R.C.J. Somerville — 1
Head, Climate Research Group, A-024
Scripps Institution of Oceanography
University of California, San Diego
La Jolla, California 92093

79. Dr. Fred Shuman, Director — 1
National Meteorological Center
World Weather Building
Washington, D.C. 20233

80. Dr. J. Smagorinsky, Director — 1
Geophysical Fluid Dynamics Laboratory
Princeton University
Princeton, New Jersey 08540

81. Dr. Andrew Staniforth — 1
Recherce en Prevision Numerique
West Isle Office Tower, 5 ieme etage
2121 route Trans-Canada
Dorval, Quebec H9P1J3, Canada

82. Dr. Mevlut Teymur — 1
Applied Mathematics Division
Marmara Research Institute
P.K. 141, Kadikoy
Istanbul, Turkey

83. Dr. W. C. Thacker — 1
National Oceanic and Atmospheric Administration
15 Rickenbacker Causeway
Miami, Florida 33149

84. Prof. Carroll O. Wilde, Code 53Wm — 1
Chairman, Department of Mathematics
Naval Postgraduate School
Monterey, California 93940

85. Dr. D. Williamson — 1
National Center for Atmospheric Research
P.O. Box 3000
Boulder, Colorado 80303

86. Dr. F. J. Winninghoff — 1
3101 Ocean Park Blvd
Sta 101
Santa Monica, California 90405

87. Dr. M. G. Wurtele 1
Department of Meteorology
University of California
Los Angeles, California 90024

88. Dr. J. Young 1
Department of Meteorology
University of Wisconsin
Madison, Wisconsin 53706

89. Prof. O. C. Zienkiewicz, Code 69Zw 1
Department of Mechanical Engineering
Naval Postgraduate School
Monterey, California 93940